pp 1153–1174. © Royal Aeronautical Society 2016
doi: 10.1017/aer.2016.48

Experimental research and numerical simulations of thrust vector control nozzle flow

S. Zivkovic
sasavite@yahoo.com
Military Technical Institute, Rocket Armament Sector
Department for Rocket Propulsion
Belgrade
Serbia

M. Milinovic
mmilinovic@mas.bg.ac.rs
University of Belgrade
Faculty of Mechanical Engineering
Department for Weapons Systems
Belgrade
Serbia

N. Gligorijevic
nikola.gligorijevic@gmail.com
Military Technical Institute
Rocket Armament Sector
Department for Rocket Propulsion
Belgrade
Serbia
Military Academy
Department for Chemical Engineering
Belgrade
Serbia

M. Pavic
cnn@beotel.rs
Military Technical Institute
Rocket Armament Sector
Department for Guidance and Control
Belgrade
Serbia

Received 12 October 2014; revised 14 January 2016; accepted 28 January 2016; first published online 25 May 2016.

ABSTRACT

Rocket motor nozzle flow geometry is considered through its influence on the thrust vector control (TVC) performances. Extensive research is conducted using theoretical and software simulations and compared with experimental results. Cold and hot flow test equipments are used. The main objective of the research is to establish the methodology of flow geometry optimisation on the TVC hardware system. Several geometry parameters are examined in detail and their effects on the system performances are presented. The discovered effects are used as guidelines in the TVC system design process. A numerical method is presented for the determination of dynamic response time upper limit for the TVC system based on the gas flow dynamics performances.

Keywords: Rocket motor; thrust vectoring; jet tabs; nozzle geometry; separated flow; recirculation zone; side force; thrust loss

NOMENCLATURE

2D	two-dimensional
3D	three-dimensional
CFD	computational fluid dynamics
TVC	thrust vector control
A_e	nozzle exit plane area
A_i	internal surfaces area
A_o	external surfaces area
A_s	shadowed area
A_t	nozzle throat area
A_0	inlet area
dT	chamber thrust
F_A	thrust loss
$\bar{F}_A$	relative thrust loss
F_B	side force
$\bar{F}_B$	relative side force
h	nozzle exit plane height
$\dot{m}$	mass flow rate
M	mass
p	pressure
p_e	nozzle exit plane static pressure
p_a	atmosphere pressure
p_0	total pressure
T	thrust
T'	pressure force
T'_x	pressure force in x-direction
V_e	nozzle exit plane velocity
x	nozzle axis direction
y^+	dimensionless wall distance
z	direction
α	nozzle expansion half-angle
γ	tab gap

https://doi.org/10.1017/aer.2016.48 Published online by Cambridge University Press

ε nozzle expansion rate
σ shadowed ratio
τ characteristic time

1.0 INTRODUCTION

Thrust vector control (TVC) is an old principle encompassing different methods for the control of rocket motor thrust force. One of these methods is generating a lateral thrust component (side force) of the rocket motor, changing the thrust vector direction[1]. The thrust vector must be precisely defined by the direction and intensity in order to generate sufficiently precise side force at the required magnitude. The TVC is useful in the cases when aerodynamic fin controls are ineffective, e.g. when extraordinary manoeuvrability is required for missiles flying at low speeds or high altitudes.

The TVC system described in the present paper is applicable in tactical missiles. The considered missile has a 'soft launch' capability and the TVC system as a nozzle exit design type, which can ensure sufficient manoeuverability at a very low launching speed, especially in the initial phase of the flight close to the ground. The considered TVC system is applied on the missile designed as a man-portable weapon, with emphasised requirements for mass optimisation[2]. The missile has a solid propellant sustainer rocket motor with a low mass flow rate and a small nozzle diameter. The jet tabs (nozzle interceptors), the jetavator (nozzle dome deflector) and the movable nozzles are motor/nozzle external thrust vectoring types of the TVC systems[3] most frequently used in these types of tactical missiles[1]. The TVC system with tabs is chosen due to the requirement for a minimum control system hinge moment, which results in the minimum design component weights in comparison to other mechanical TVC systems[1,4]. Despite these advantages, it has a low efficiency of the side force generation when compared to thrust intensity losses[1].

The TVC characteristic values and their interdependency with the geometry parameters are examined in many theoretical and experimental research works[5]. According to the works mentioned, this type of TVC systems generates a maximum value of side forces, when the exit area of the nozzle is shaded by the tabs for nearly 50%. Gas-dynamic drag during the motion of the tabs through the nozzle jet is minimal when the tab surface is perpendicular to the nozzle axis. In such conditions, the expected thrust loss could be higher than 30% of the nominal (undisturbed) thrust[6]. In this particular case, in flight conditions that dictate the frequency of the TVC use, total impulse losses can be higher than 20%. The mass of the propellant is about 20% of the total missile mass, so an additional amount of propellant could be required to compensate for the total impulse losses[7]. This leads to the conclusion that the TVC system applied here is not the best with respect to losses, but is still the best regarding the mass ratio of subsystems and components.

During the combustion products expansion through the nozzle, inflicted at the exit area by the insertion of a jet tab, complex disturbed flow inside the supersonic area is generated. The correlation between the gas dynamics and the geometry parameters of the disturbed flow domain and its effects on the thrust vector direction inclination is stressed in the present paper. In order to maximise the efficiency of this type of TVC system, extensive research of the influence of geometry parameters on thrust vectoring was carried out and published earlier by Jojic[5] and Zivkovic[6]. The initial examination of the gas dynamic phenomena related to internal flow separation caused by obstacles in the supersonic stream given in those papers is conducted in the supersonic wind tunnel presented in several papers[5, 8, 9]. Based on

https://doi.org/10.1017/aer.2016.48 Published online by Cambridge University Press

these experimental results, reliable CFD simulations are developed, as described in papers by Gligorijevic[7], Kozic[8] and Zivkovic[6, 9], in order to confirm the existing development stage and to facilitate further development of the TVC systems.

2.0 GAS DYNAMIC PERFORMANCES OF SEPARATED FLUID FLOWS

Inserting a tab as an obstacle in a supersonic stream generates an oblique shock wave upstream and a high-pressure recirculation zone below the wave. The supersonic flow downstream the oblique shock wave shapes the recirculation zone in a form of a liquid wedge between the separation point and the top of the tab profile[10], Fig. 1. At the top of the wedge, the boundary layer is separated downstream and the pressure is redistributed, generating an additional pressure force on the nozzle walls and inflicting summary thrust vector direction inclination. The side force depends mainly on the size and the level of the redistributed pressure in the recirculation zone (Fig. 2). On the other hand, thrust losses depend mainly on the size of the part of the nozzle exit plane covered with the jet tab—the so-called shadowed area A_s (Fig. 1).

A basic task for the TVC system design is to generate a side force with required intensity and duration based on the explained principles. The best performance of the system is obtained when thrust losses are minimal for the required values of the side forces. The optimum TVC system performances can be determined using the two characteristic values, the side force intensity and the thrust loss, which have to be taken as the prime optimisation criteria:

1. The required value of the generated side force F_B, which can be represented as the relative side force, as a ratio to the mean thrust T: $\bar{F}_B = F_B/T$;
2. The minimum counter-thrust defined as the thrust loss F_A, which can be also expressed as the relative thrust loss: $\bar{F}_A = F_A/T$.

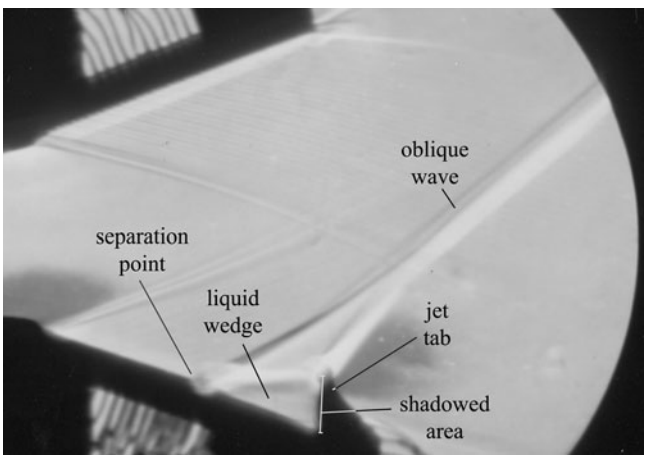

Figure 1. Schlieren photography of the two-dimensional nozzle with the tab in the wind tunnel during the cold flow test.

https://doi.org/10.1017/aer.2016.48 Published online by Cambridge University Press

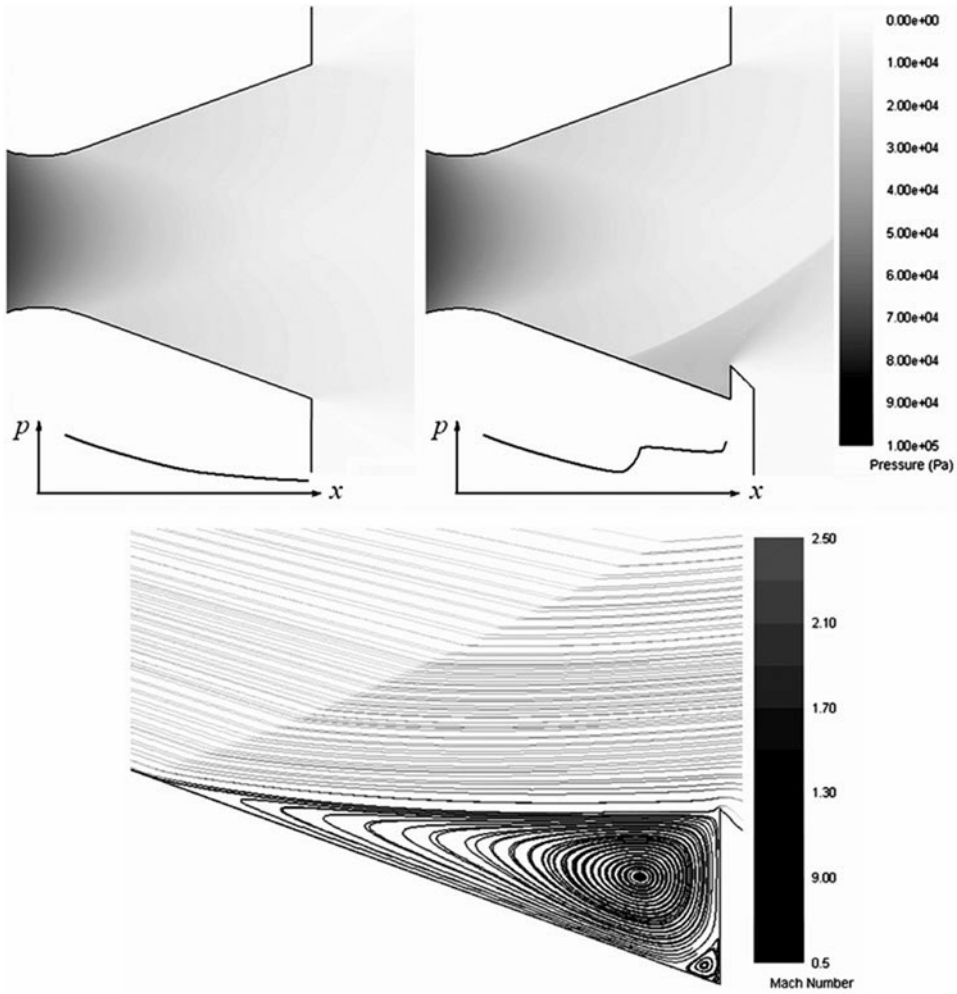

Figure 2. CFD simulation of the two-dimensional cold flow test. Pressure contours and typical pressure distribution on the nozzle lower wall in the nozzle without (left) and with jet tab (right). Streamlines in the recirculation zone (below).

The first step in this research is to discover and evaluate the influence of flow separation and pressure distribution, and to determine the main parameters that could be taken as design elements for the TVC integration with the nozzle as a flow source.

3.0 EXPERIMENTAL AND NUMERICAL RESEARCH OF THE TWO-DIMENSIONAL COLD FLOW

Some of the results from earlier wind-tunnel examinations will be presented in this section to illustrate cold flow gasdynamic phenomena, which is important for the actual research. The experimental model with a test bed, in the test section of the wind tunnel, is shown in Fig. 3. In these cold flow tests, the atmospheric air is used as the working fluid, driven by the

https://doi.org/10.1017/aer.2016.48 Published online by Cambridge University Press

vacuum tank at the rear end of the wind tunnel. During increasing of the pressure level in the outlet vacuum tank, from 5 mbar to 50 mbar, the expected testing process was running. Mach numbers of the two tested nozzles were 2.3 and 2.6, with expansion rates values of 1.9 and 2.9, respectively, and both nozzles were under-expanded. Reynolds numbers in those two cases were 9.7E6 1/m and 1.1E7 1/m, respectively. Generally, turbulence of incoming supersonic flow has a strong influence on the separated flows, as stated by Chang[10]. He reported that shock waves shape, position, pressure distribution and diversification of boundary layers into the sublayers depend on incoming Re numbers. On the other hand, Ostlund[11] described the separation mechanism as insensitive at high Re numbers larger than 10^5. In those conditions, the author stated, the separation point and pressure distribution in the recirculation zone are dependent only on the incoming Mach number. This is also accepted as the assumption in the present paper.

In the cold flow tests, in the divergent part of the nozzle, relatively low static temperature of air (about 150° K) is expected. This is moderate difference, relative to nozzle walls temperature, but heat transfer on the nozzle walls can be neglected, because of the short time exposition during the experiment.

The flow visualisation is enabled with a two-dimensional model of convergent-divergent nozzle with one tab at the exit plane. The shadowed area is principally a segment of the exit area blocked by the involved stream obstacle. Changes in the values of this area are achieved simply by replacing the obstacle position normal to the main stream flow referred to the nozzle axis (Fig. 3). The basic gas dynamic processes are identified and pressure distribution is measured in the separated flow, formed as the recirculation zone. Some relationships can

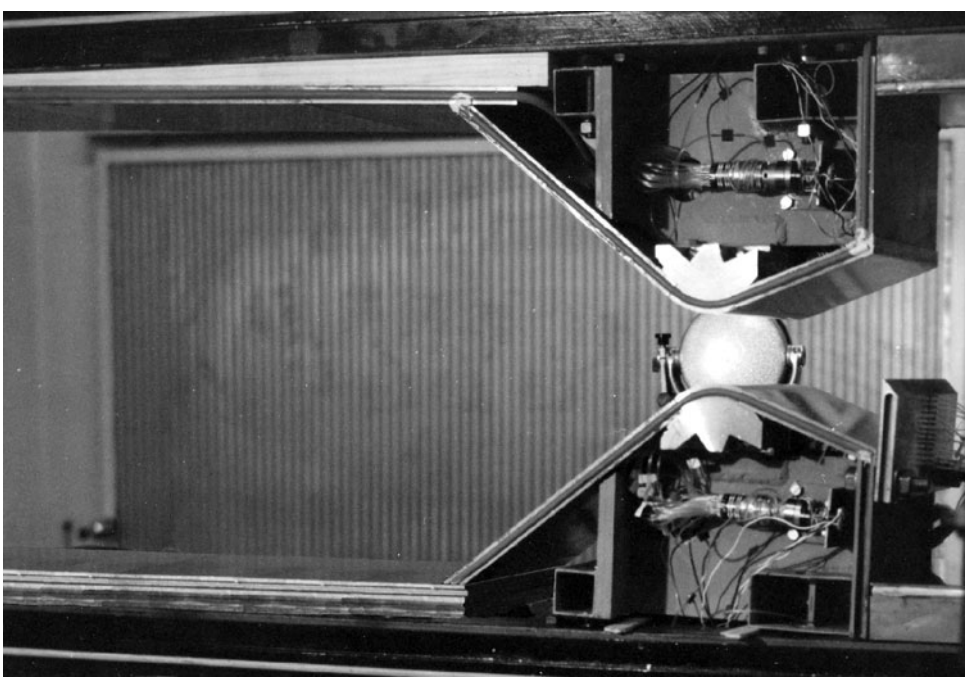

Figure 3. Experimental model in wind-tunnel test chamber for the two-dimensional cold flow test.

https://doi.org/10.1017/aer.2016.48 Published online by Cambridge University Press

be successfully explained by analysing the Schlieren photography from these experiments (Fig. 1). Based on these experiments, further conclusions can be made:

- Geometry parameters of the divergent supersonic part of the nozzle, together with the tab position, define the recirculation zone shape, size and pressure distribution. Consequently, these parameters have the strongest influence on the effects of the side force generation.
- The shadowed area is the most influential geometry parameter in terms of the recirculation zone size and the generated shock wave position. Increasing the shadowed area increases the recirculation zone size. The shadowed area influence depends on the incoming flow parameters such as Mach number, expansion level, etc. This is noticeable in the test with the nozzle expansion ratio variation (to be explained below).
- The boundary between the recirculation zone of the supersonic stream beyond the oblique wave stretches between the top point of the tab and the separation point of the boundary layer on the nozzle surface (see Fig. 1). Some successful empirical correlations, such as the characteristic point position in the recirculation zone and pressure distribution, are given by Schilling[12], Jojic[5] and Waithe[13].

The observations in these experimental researches were verified by the two-dimensional CFD simulations with the FLUENT program by Kozic[8] using the k-ω turbulent model. Tian[14] reported better performances of the Goldberg's k-ε-Rt model, and Balabel[15] found best performances for similar applications using the transport SST turbulence model, with respect to experimental data. A new CFD testing in FLUENT for two-dimensional TVC nozzle experiments, provided by Zivkovic[9], also confirmed most of the mentioned conclusions. In those simulations, the SEGREGATED solver is used with the SIMPLE algorithm and second-order upwind discretisation schemes—terminology taken from[16]. The transition SST turbulence model is proved to be the best one for this type of gas flow. This turbulence model is designed to better resolve the transitional processes which lead to the boundary layer separation[16].

Figure 2 shows the particular flow regions observed in the CFD test. The following conclusions can be drawn from the simulation, based on the experimental flow measured data:

- The boundary of the recirculation zone is slightly curved under the supersonic flow downwind of the oblique wave due to the pressure balance of the supersonic stream and the recirculation zone.
- One large and several smaller eddies in the main and secondary recirculation zones are created under the influence of the viscous forces on the boundary of supersonic main flow and recirculation zone stream. Only a few largest eddies are clearly visible in Fig. 2.
- The velocity in the recirculation zone is subsonic and much lower than the velocity in the supersonic stream.
- Jojic[5] stated that for two-dimensional nozzles and for one type of gas, the pressure level in the recirculation zone is approximately constant (the plateau pressure, as also denoted by Chang[10]), and depends only on the pressure and the Mach number at the separation point.

Two-dimensional cold flow tests also show approximately constant pressures in the recirculation zones on the nozzle surfaces (Fig. 4). This is expected because the flow velocity

https://doi.org/10.1017/aer.2016.48 Published online by Cambridge University Press

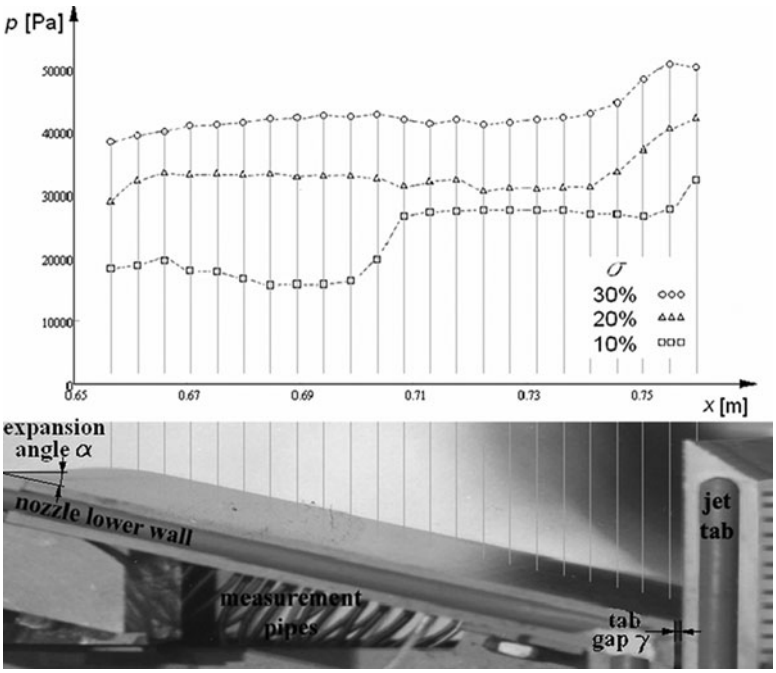

Figure 4. Shadowed ratio influence on the pressure distribution on the lower nozzle wall in the two-dimensional cold flow test (diagram above) and lower nozzle wall configuration (below).

in the recirculation zone is low, and a static pressure level is mainly defined by the shock wave as well as by the vortices total pressure losses[5]. Figure 4 shows the pressure distribution (p) at the lower nozzle side, along the nozzle axis position (the x-axis), measured in the experiments, as presented by Zivkovic[9]. The results are displayed for three experiments, with 10%, 20% and 30% of the shadowed area A_s relative to the nozzle exit area A_e (the shadowed ratio $\sigma = A_s/A_e$). The lowest curve matches the experiment with the 10% shadowed ratio. The separation point is positioned in vicinity of the middle of the nozzle length. Pressure decreases during expansion, and after the separation point, it suddenly jumps to a constant level in the recirculation zone (plateau pressure). In the other two experiments, the separation point is positioned upwind of the first measured point and both other curve levels correspond to the estimated plateau pressure in the recirculation zone. As expected, the plateau pressure increases with a higher level of the shadowed ratio.

The appearance of a gap between the tab and the nozzle exit plane (the tab gap γ in Fig. 4) also has an effect on the recirculation zone position, which is similar to the effect of the shadowed ratio decrease. This could be an important performance criterion for the thrust vector control system design. Based on the earlier experience with the rocket motor TVC system operation, problems related to the small tab gaps due to thermal dilatation and the combustion products condensation are expected. The larger tested values of relative gaps in the 2D simulations and experiments are examined with the aim of obtaining a broader perspective on the tabs using and the process understanding. Increasing the gap moves the separation point position towards the exit plane, and the pressure level decreases (Fig. 5) due to gas leaking through the gap, i.e. the gap ejects the mass from the recirculation zone. This is the most important experimental conclusion obtained from the final presented data. The mass

https://doi.org/10.1017/aer.2016.48 Published online by Cambridge University Press

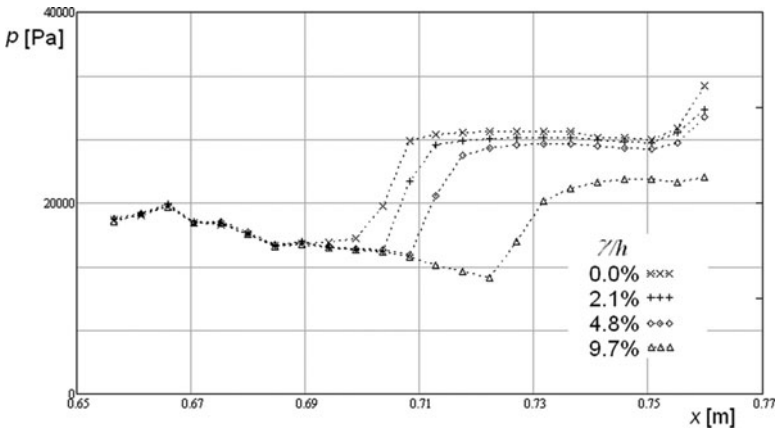

Figure 5. Gap influence on the pressure distribution on the lower nozzle wall in the two-dimensional cold flow test.

flow rate through the gap is proportional to the gap size, and it is evident from Fig. 5 that the plateau pressure and separation point position will be also proportional to it. The comparison between the experiments with different expected gaps is shown in Fig. 5. The values of the gaps are expressed by the gap-to-exit-plane height h ratio.

The convergent-divergent nozzle expansion rate $\varepsilon = A_e/A_t$ (the nozzle exit to the throat area ratio) and the expansion half-angle α (Fig. 4) also have significant influence on the recirculation zone. Experimental research in the cold flow tests includes the comparison between two values of the expansion rates 1.9 and 2.9. Comparing those two nozzle configurations at the same shadowed ratio 10% and then at 30%, the nozzle with a lower ε has higher plateau pressure in both cases (Fig. 6). Comparing curves with 10% shadowed ratio as a more obvious case, the curve for the 1.9 expansion rate has a higher pressure level in the entire divergent part of the nozzle; consequently, the separation point pressure will be also higher. As mentioned, this leads to a higher value for the plateau pressure and the separation point position is closer to the nozzle throat (Jojic[5]). Generally, in nozzles with lower expansion rate values, higher plateau pressure values can be generated, and it is considered to be closer to the optimum configuration.

For the determined gas flow parameters, the considered geometry parameters of the flow domain influencing the separation point position and the recirculation zone shape in the present research are:

- shadowed ratio – σ;
- tab gap – γ;
- nozzle expansion ratio – ε.

Wind-tunnel test equipment does not allow for direct thrust components measurement. The main purpose of this type of research is the analysis of separated flow phenomena. Hypothetically, the expected side force could be calculated like the pressure integral of the recirculation zone area, as a component perpendicular to nozzle axis direction. Axial components of the thrust cannot be calculated from the measured pressure profiles. The measurement of the thrust force components and effects of the mentioned parameters on

https://doi.org/10.1017/aer.2016.48 Published online by Cambridge University Press

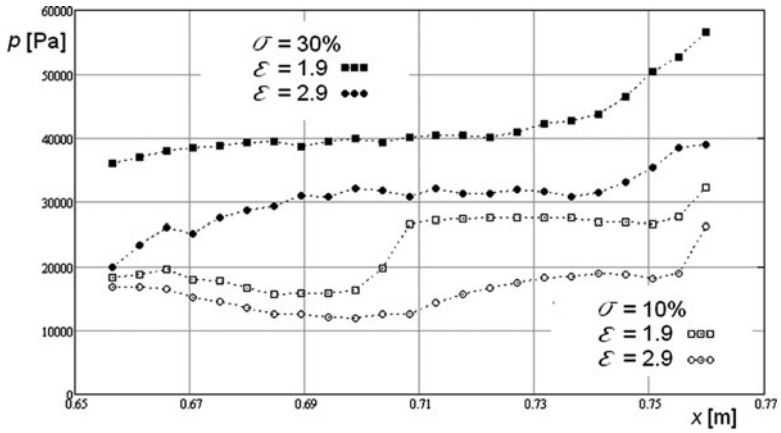

Figure 6. Expansion rate influence on pressure distribution on the lower nozzle wall for two values of the shadowed ratio in the two-dimensional cold flow test.

the side forces and thrust losses were tested on the three-dimensional nozzle geometry. The research is realised by the three-dimensional tests equipment and qualitatively compared with above described two-dimensional cold flow tests.

4.0 THREE-DIMENSIONAL EXPERIMENTAL TEST EQUIPMENT

The second phase of the research was conducted with an experimental three-dimensional TVC system with the flow domain geometry similar to the missile[6]. The experimental system is designed to enable a large number of experiments and to vary different design parameters within their threshold origins and values.

The variable parameters influencing the performances are:

- shadowed ratio – σ;
- tab gap – γ;
- nozzle expansion ratio – ε;
- nozzle expansion half-angle – α.

The experimental three-dimensional test equipment is shown in Fig. 7, and main components of this system are:

- six-component test stand, with the acquisition system;
- experimental demo rocket motor;
- experimental TVC system with the command system;
- air supply installation for cold flow tests;

and appropriate components such as nozzles, transducers, encoders, etc. shown in Fig. 7.

The measurements provided data with the next estimated accuracy level:

https://doi.org/10.1017/aer.2016.48 Published online by Cambridge University Press

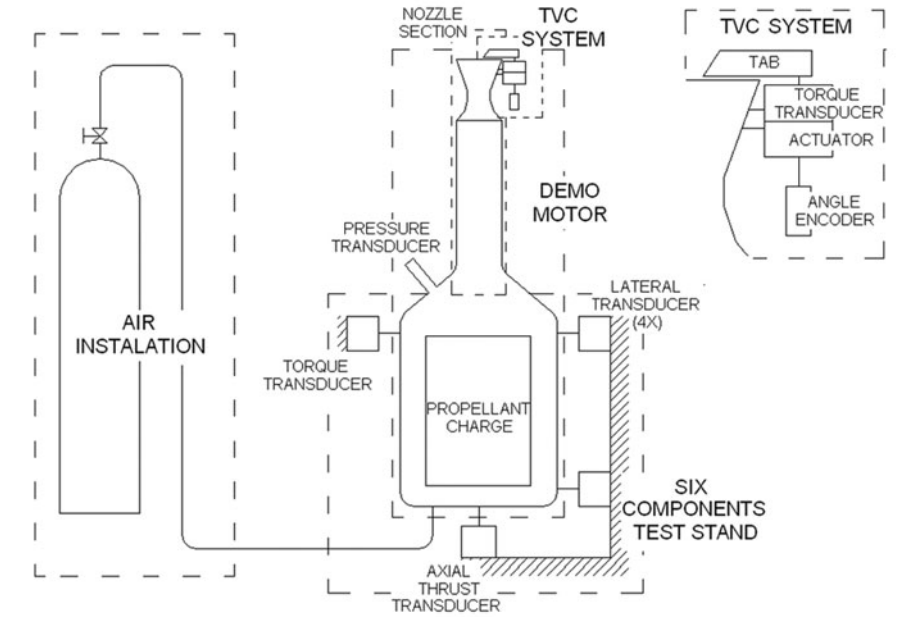

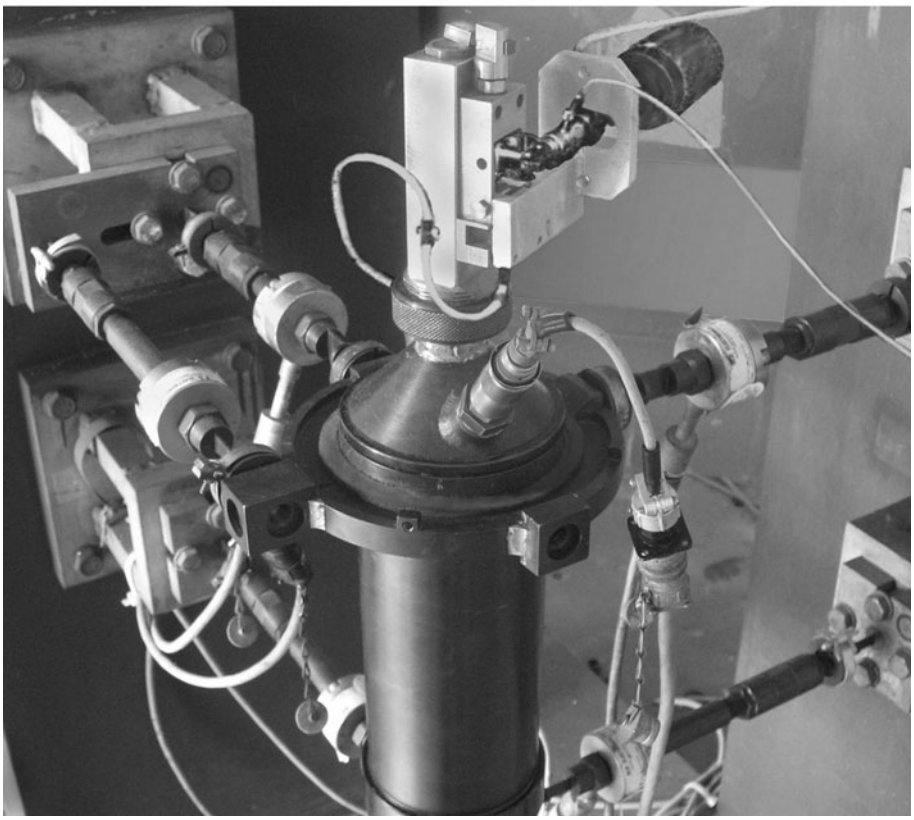

Figure 7. Experimental equipment for three-dimensional tests (below) and functional scheme.

https://doi.org/10.1017/aer.2016.48 Published online by Cambridge University Press

- thrust components: accuracy of 0.5% for thrust and 1.5% for side force;
- total pressure in the chamber: 0.5% accuracy;
- the tab position: 1.5% accuracy;
- drag of the tab motion through the jet as measured by the torque transducer: 1.5% accuracy.

The system operates optionally as a cold or hot test installation with the same flow geometry. Preliminary performances are selected by cold flow tests, using the high pressure air. The hot flow tests are conducted using combustion products provided by the demo rocket motor with double-base solid propellant charges.

Six component loadings of thrust vectoring are measured, three components of the force and three components of the moment, which are calculated using data from the test stand designed for simultaneous data collecting of the thrust vector intensity and the vector space position[7]. The nozzle section of the demo motor provides a variation of different nozzle geometry parameters: the expansion ratio and the angle of expansion. The experimental TVC system is attached to the nozzle section of the demo motor. The tab support allows axial positioning for the tab gaps testing. The tab operates by a controlled angular motion from the zero position (out from the jet of the nozzle) to a threshold up to 0.5 of the shadowed ratio. The shadowed ratio is part of the blocked exit area made by the tab, which is a circular segment of the exit nozzle surface determined by the tab penetration depth into the main stream. Angular motion of the tab provides required penetration depth and proportional values of the shadowed exit area. This requires a measuring transducer: an angular encoder that controls these values regarding the nozzle and tab geometry with appropriate software and hardware. The tab makes angular motions within given angles and opens the shadowed exit nozzle area. The mean values of the thrust and the side force are adopted from the tab operating cycles.

5.0 THREE-DIMENSIONAL EXPERIMENTAL RESULTS AND ANALYSES

During this research, most of the conducted experiments involved cold flow tests. In the experiments, the air pressure in the RM chamber is maintained at constant level of about 35 bar and the corresponding mass flow rate trough nozzle was about 0.31 kg/s. Estimated flow Reynolds number is 1.7×10^7 regarding semi-empirical calculation for the rocket motor geometry by Dobrovolskiy[17].

The geometry parameters, which are varied in the cold and hot flow tests within the following ranges of significance for this analysis, are:

- $\sigma = 0$ to 0.45;
- $\gamma = 0$–0.5 mm;
- $\varepsilon = 3$, 4.7 and 6.8;
- $\alpha = 12°$, 15° and 20°.

Figure 8 shows the results from six experiments of the shadowed ratio effects on the trust losses and the side force. Different gaps were discovered on the two used types of nozzles; for half-angles of the nozzle divergence $\alpha = 12°$ (Fig. 8(a)), and for $\alpha = 20°$ (Fig. 8(b)), both

https://doi.org/10.1017/aer.2016.48 Published online by Cambridge University Press

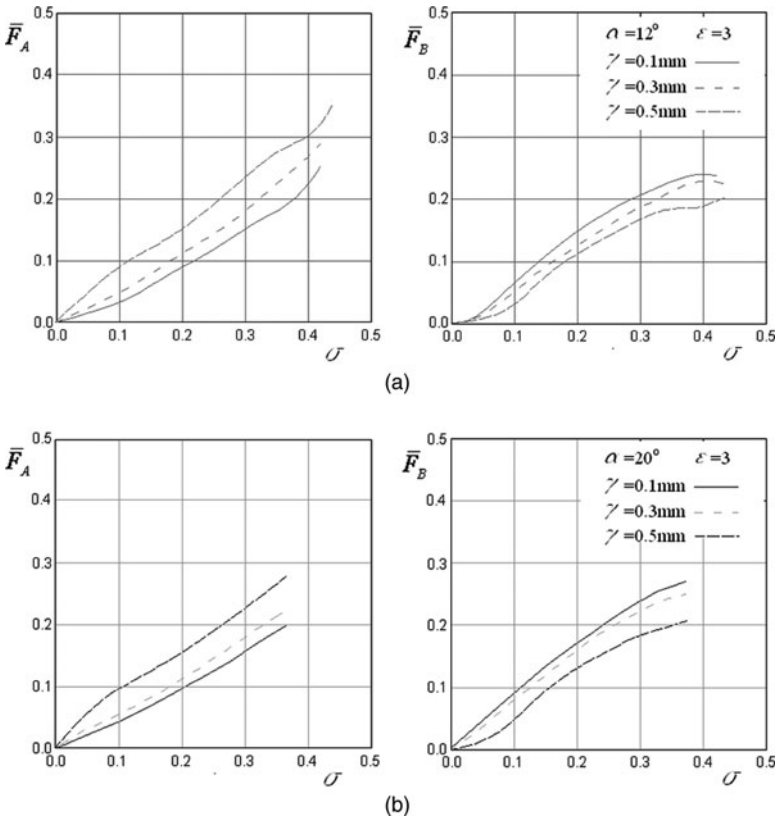

Figure 8. Shadowed ratio influence on the trust losses and the side force for different gaps and two values of divergence half-angles.

with the expansion ratio $\varepsilon = 3$. The goal of the experiments was to test the influence of the designed values of the gaps of 0.1 mm, 0.3 mm and 0.5 mm, obtained by tab operations, on the generated loading in the continual process of exit area shadowing. The experiments confirm that the decrease of the tab gap value for the same shadowed ratio produces the increase of the side force. This is in accordance with the two-dimensional experiments presented in Fig. 5. The plateau pressure in the separation zone is highest for the zero tab gaps, which produces the best generation of the side force. The thrust loss is more significant with increasing tab gaps (Fig. 8).

Figure 9 shows the results from nine experiments of the shadowed ratio effects on the thrust losses and side forces, with the expansion ratio variation values of 3, 4.7 and 6.8 for three different divergence half-angles of the nozzle. Larger expansion rates show smaller side force values and smaller thrust losses as a function of the shadowed ratio. Increasing the nozzle expansion half-angle from 12° (Fig. 9(a)) to 15° (Fig. 9(b)) diminishes this difference and, at a half-angle of about 20° and greater (Fig. 9(c)), it could be expected that the effect of the nozzle angle increase 'throttles' the expansion rate influence on the side force, analogous to the case of the thrust loss. The principle and the basic 2D conclusions about the generation of higher side thrust forces with a lower expansion ratio (Fig. 5) are proved in these 3D experiments.

https://doi.org/10.1017/aer.2016.48 Published online by Cambridge University Press

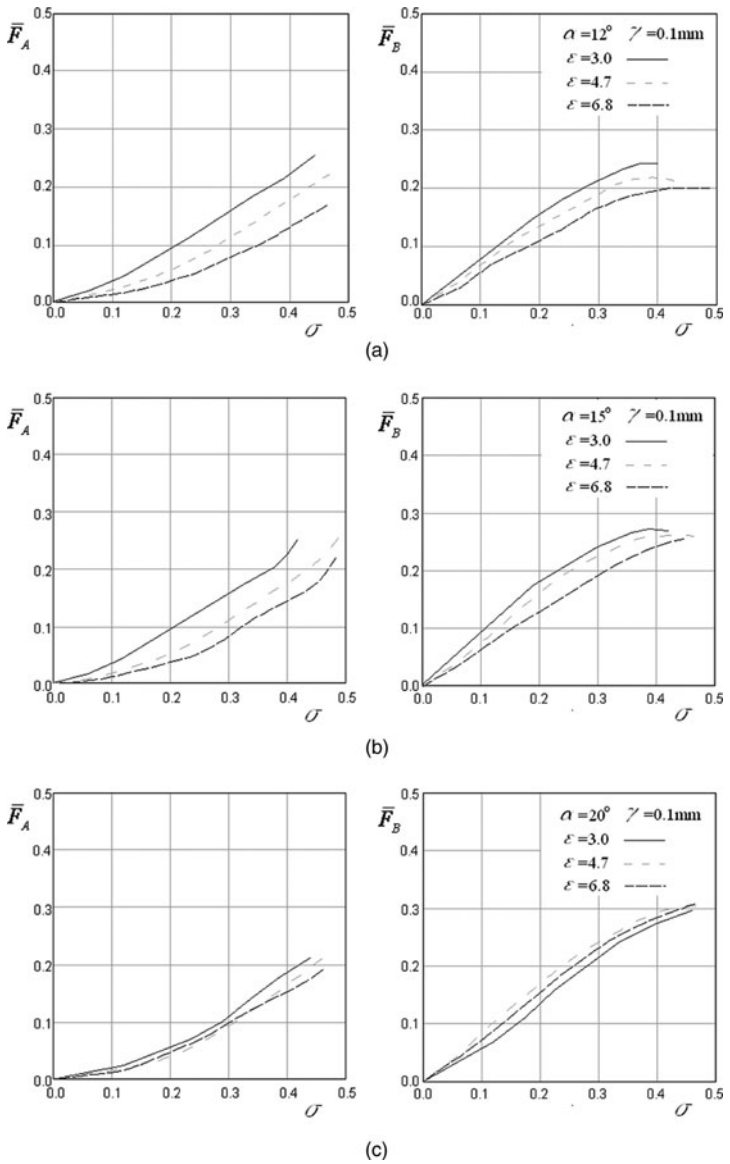

Figure 9. Shadowed ratio influence on thrust losses and side force for different expansion rates and three values of divergence half-angles.

In Fig. 10, a variation of the same basic function of side forces and thrust losses vs the shadowed area is realised by a variation of the nozzle expansion half-angles from 12°, 15° and 20° given for two nozzle expansion ratio values of 3 and 6.8 (Fig. 10(a) and (b), respectively). The side force generally increases with the increase of the half-angle, and the thrust loss is almost insensitive to this change. These results conform to the conclusion about thrust losses discovered in the previous result, shown in Fig. 9, namely that thrust losses are higher at the lower expansion rates. Side forces are less sensitive to the nozzle expansion

https://doi.org/10.1017/aer.2016.48 Published online by Cambridge University Press

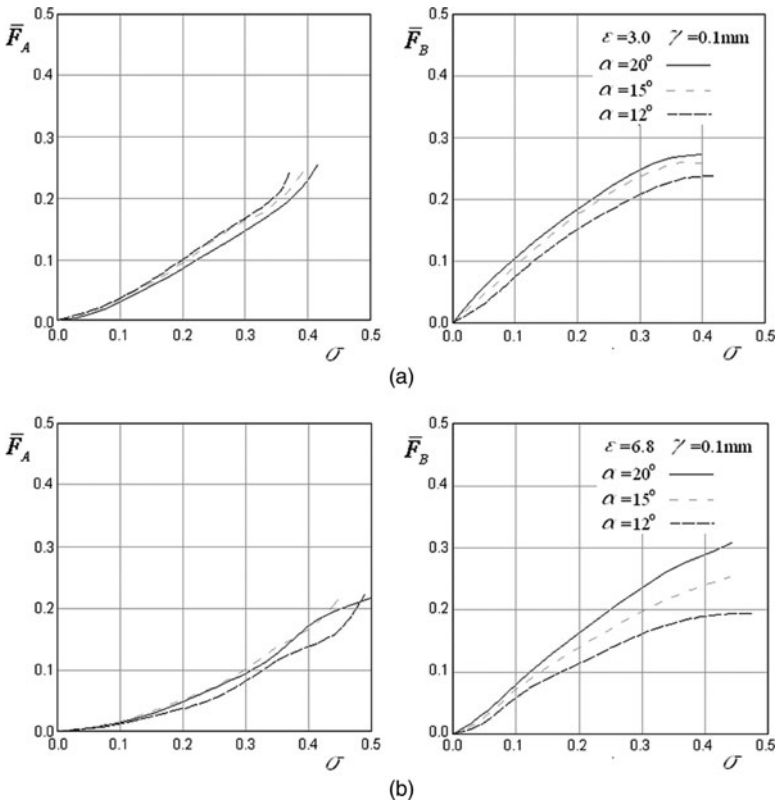

Figure 10. Shadowed ratio influence on the thrust losses and side force for different half-angles of divergence and two values of the expansion rate.

angle change at a lower expansion rate (value 3, Fig. 10(a)) than at a higher one (value 6.8, Fig. 10(b)).

6.0 CFD SIMULATIONS AND TESTS ANALYSIS

In order to evaluate the quality and quantity of the forces generation processes of a TVC system, additional CFD simulation tests are performed on selected influencing parameters discovered in the mentioned research works as optimal and applicable for a real missile TVC system. The three-dimensional CFD simulation is conducted using the FLUENT program. The model geometry similar to three-dimensional experimental nozzle and the TVC system elements are shown in Fig. 11, prepared for the quasi-steady-state calculation by changing of appropriate geometry parameters. Dynamical CFD testing was not performed.

The CFD simulation is verified by the comparison with the three-dimensional experiments with the nozzle geometry parameters of $\alpha = 20^{o}$, $\varepsilon = 3$ and $\gamma = 0.3$ mm. Based on the experience with simulation of two-dimensional tests, the same calculation parameters are used: SEGREGATED solver with the SIMPLE algorithm, second-order upwind discretisation schemes and the transition SST turbulence model.

https://doi.org/10.1017/aer.2016.48 Published online by Cambridge University Press

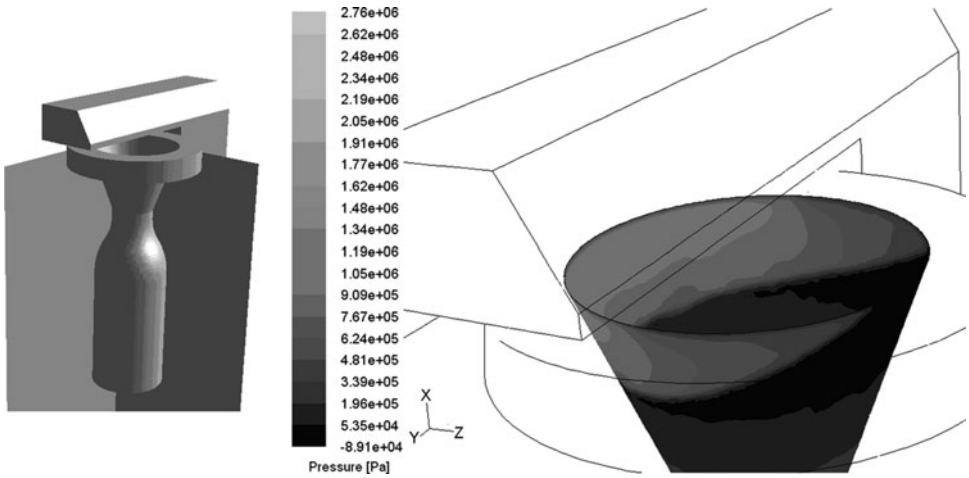

Figure 11. CFD model geometry and the pressure distribution on the inner surface of the nozzle.

Pressure distribution on the nozzle internal walls is presented in Fig. 11. Effects of three-dimensionality, such as conically curved shape of recirculation zone, are noticeably conditioned by the conical nozzle wall. The jet tab position generates shock waves covering almost the entire nozzle exit surface in position to generate the maximum available side force.

The 'pressure inlet'[16] boundary conditions are deployed in simulations: total pressure 28.3 bar, as a mean value of chamber pressure, measured in the experiments; and total temperature 300°K. Necessary turbulence parameters at inlet are chosen as recommended by the FLUENT user's guide[16]: the intensity level is 2% estimated by mentioned Dobrovolskiy's[17] equation, the hydraulic diameter equal to the inlet diameter is 12.5 mm, and the intermittency factor is 1.

The sphere around the nozzle exit and TVC elements, whose diameter is ten times larger than the nozzle exit diameter, is chosen for the "pressure outlet"[16] boundary. FLUENT default backflow atmospheric values are chosen at the outlet: standard pressure level, temperature 300°K, turbulence kinetic energy $1\,m^2/s^2$, specific dissipation rate $1\,s^{-1}$ and intermittency factor 1.

All other surfaces of the model are the walls, with the default roughness parameters and negligible heat transfer flux.

In the transition SST turbulence model, the boundary layer flow can be calculated applying wall functions or enhanced wall treatment[16]. Using fine mesh resolution with the y^+ level close to one is preferable for highly accurate modelling of boundary layers, including precision prediction of laminar-turbulent transition. In two-dimensional geometry, it is fairly easy to fulfil this requirement, as well as in simple three-dimensional cases as described by Jaunet[18] or Zmijanovic[19]. However, in a more complex three-dimensional geometry grid generation, it is very hard to fulfil the recommendations with moderate mesh sizes and acceptable computational cost, as with geometry presented by Tian[14]. The advantage of the SST turbulence model is the flexible approach of near wall treatment using wall function or enhanced wall treatment model. During the iterative process, the solver calculates the local values of y^+ based on the grid size, flow parameters and fluid properties. The interdependency of y^+ value software makes the decision which approach will be used. Less accurate estimation

https://doi.org/10.1017/aer.2016.48 Published online by Cambridge University Press

Table 1
Grid dependency testing results

Total cell number	Boundary layer cell levels	y^+	Side force (N)	Thrust loss (N)
64,000	1	200	39.76	46.12
510,000	2	100	41.16	46.47
4,100,000	4	50	40.58	47.44

of boundary layers separation process is expected with wall functions approach than for the enhanced wall treatment models[16].

The grid dependency is tested on a coarse mesh with about 64,000 cells in a divergent part of the nozzle. The achieved dimensionless wall distance y^+ level in the recirculation zone is over 200, the nozzle gap is resolved with four layers of cells, and almost the entire boundary layer is placed in the first row of the cells adjacent to the nozzle walls. Using the adaptation technique in FLUENT, every cell in this zone is divided into four cells. A new mesh has about 510,000 cells in a divergent part of the nozzle, and has y^+ level about 100. In the final refinement step, the mesh has 4,100,000 cells and a y^+ level of about 50. During calculation, a very low level of residuals is achieved in all models: for turbulence governing equations nearly 10^{-4}, and for other equations even lower than 10^{-5}. Table 1 gives calculated values of the side force and thrust losses in those three cases. There is no large difference between the results for all three models, so it can be concluded that mesh is acceptable in all those cases.

The calculation procedure for the thrust, side force and thrust loss components is based on the standard grid numerical integration in the FLUENT program. The calculation of the thrust components is conducted using force determination as the pressure integral on the nozzle, the jet tab and the motor walls. The side force and the axial thrust are calculated as the pressure force integral components in the z direction and the x direction, respectively (Fig. 11). The computational procedure is described by Zivkovic[6]. The calculation is based on the 'thrust definition approach'[6] using the 'force report' tool for pressure force calculation in the FLUENT as:

$$T' = -\left(\int_{A_i} p d\vec{A} + \int_{A_o} p d\vec{A}\right) = -\left(\Sigma p A_i + \Sigma p A_o\right), \quad \ldots (1)$$

where motor internal surfaces area is A_i, and external surfaces area is A_o.

As described in the above-mentioned paper, the thrust components can be calculated using the so-called reduced geometry model, where the combustion chamber flow domain is omitted and only the nozzle section and the TVC flow space are considered (Fig. 12). A calculation of undisturbed thrust can be provided using the 'classical approach' by the equation:

$$T = \dot{m} V_e + (p_e - p_a) A_e, \quad \ldots (2)$$

where mass flow rate is $\dot{m}$, mean axial nozzle exit plane velocity is V_e, mean nozzle exit plane static pressure is p_e, atmosphere pressure is p_a and nozzle exit plane area is A_e.

https://doi.org/10.1017/aer.2016.48 Published online by Cambridge University Press

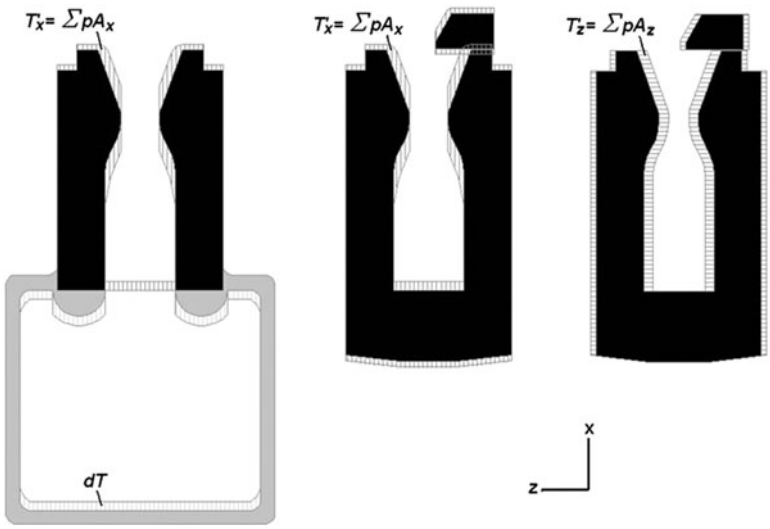

Figure 12. Scheme of the 'thrust definition approach' calculation method using the reduced geometry model.

Using the 'thrust definition approach' on a reduced model, a lower value of the thrust will be obtained using Equation (1) (pressure force in the x-direction T'_x – Fig. 12, left), compared to the result obtained with Equation (2), because there is always the pressure force component generated in the combustion chamber-chamber thrust that increases thrust intensity:

$$dT = T - T'_x \qquad \ldots (3)$$

Finally, thrust loss can be calculated using a simulation with reduced geometry based on the next equation (Fig. 12, middle):

$$F_A = T - \left(T'_x + p_0 A_0 + dT\right), \qquad \ldots (4)$$

where chamber total pressure is p_0, flow domain inlet area is A_0.

Calculation of the side force is simpler. Because of the symmetry of combustion chamber, the lateral component of the chamber thrust does not exist in the omitted geometry. The intensity of the side force can be calculated using the force report tool in the z direction directly (Fig. 12, right):

$$F_B = T'_z \qquad \ldots (5)$$

Comparing the results of CFD simulations and experiments (Fig. 13), relatively good agreement is achieved, with an error of several percent in the relative side force and thrust loss estimations.

https://doi.org/10.1017/aer.2016.48 Published online by Cambridge University Press

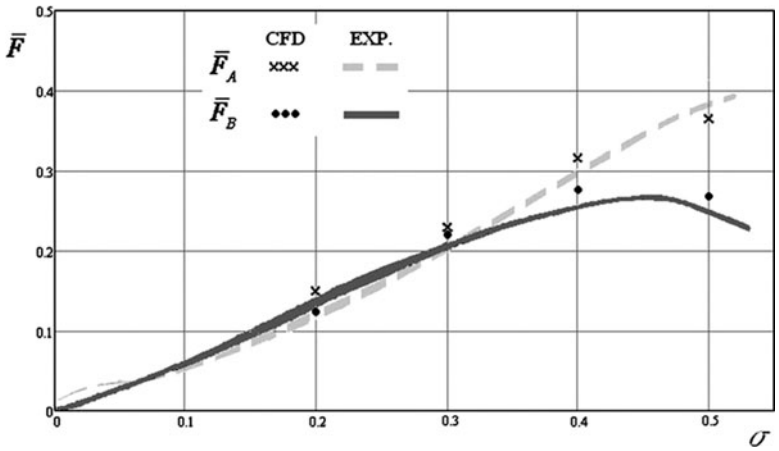

Figure 13. Shadowed ratio influence on the thrust losses and side force, correlation between the experiments and the CFD simulation.

7.0 DYNAMIC PERFORMANCES OF THE SEPARATION ZONE IN THE REAL THRUST VECTOR CONTROL VARIATION

In this part of the research, the dynamic behaviour of separation flow changes was tested in order to find an optimum ratio between the frequency of tab swings and the dynamic response of the separation effect caused by the shadowing of the exit nozzle area. The main performance of the inertial behaviour of the separated recirculation zone in the nozzle is its time response, determined by the nozzle flow performances and an appropriate mass of gas captured in the circulation vortex of the recirculation zone (Fig. 11). The main time characteristic expresses the change of mass in this volume after one tab opening and is taken as a frequency of the gas-dynamic reaction on the tab position changes caused by swinging in the real TVC operation. In Fig. 14, the real-time characteristic of gas flow changes is compared against the frequency period of tabs operation in the real missile. The CFD program calculated the values of the characteristic time:

$$\tau = \frac{M}{\dot{m}}, \qquad \ldots (6)$$

where M is the mass of the captured gas in the separation zone calculated for the plateau pressure and for other state values of gas and $\dot{m}$ is the mass flow rate of products in the rocket motor.

Figure 14 shows the changes of characteristic times vs shadowed ratio. The characteristic time of the gas flow is higher by more than two orders of magnitude than the calculated limit of mechanical systems with tabs, which leads to the conclusion that TVC could be successfully applied as a side force generator in real missile guidance conditions.

Thanks to a low hinge moment, this type of TVC has a more rapid dynamic response than other mechanical systems. The measured dynamic response on a real missile TVC is about 30 Hz, which is a high-end performance for mechanical systems in general[20].

https://doi.org/10.1017/aer.2016.48 Published online by Cambridge University Press

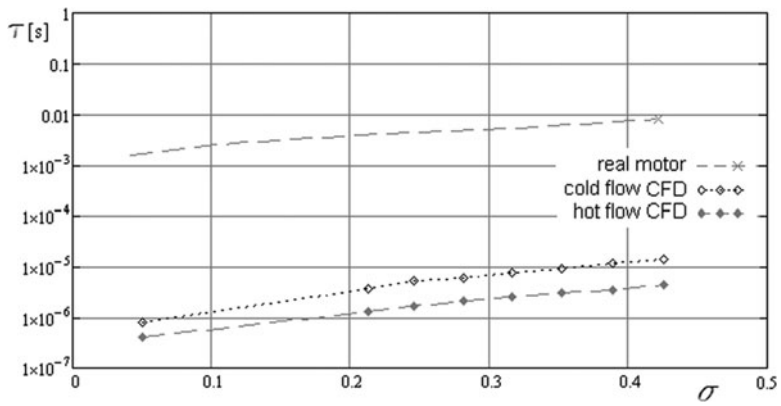

Figure 14. Shadowed ratio influence on characteristic time of the gas flow process and the mechanical tab system operation ($\gamma = 0.1$, $\alpha = 20°$, $\varepsilon = 3.0$).

8.0 DISCUSSION

Some interesting effects of the variable geometry parameters of flow domains on the TVC performances are verified in experiments and compared against numerical simulations.

On the basis of the experimental results, it is proved that the most influencing geometry parameter on the side force generation is the shadowed ratio. A higher shadowed ratio brings the separation point closer to the throat, which means it is positioned at higher static pressures. The plateau pressure level in the recirculation zone is proportional to the static pressure in the separation point[5]. It is possible for the generated shock wave to cover the entire exit area and decrease the exit velocity, thereby reducing the thrust force (Fig. 11). In these cases, the maximum side force is achieved and further shadowing is ineffective[6]. Also, the shock wave sliding over the boundary layer could touch the throat, thus making a chocking effect in an extreme case. As for thrust losses, they depend on the nozzle flow disturbance, which occurs during a TVC process in the divergent part of the nozzle. A part of the stream lines is deflected in a direction different from the nozzle axis, and as a result the thrust force is decreased. In addition, the velocity of the flow is reduced after the transit through the shock wave. In TVC systems with tabs, the size of the tab surface interacting with the recirculation flow has the greatest influence on thrust loss (Fig. 11).

The level of pressure in the recirculation zone depends largely on the distance between the tab and the nozzle; this distance represents a gap through which fluid flow leaks, resulting in the plateau pressure decrease in this zone. The pressure drop is proportional to the gap size and is more significant with a larger gap increase (see Fig. 5). But even with a smaller gap increase, the separation point moves closer to the tab, so the summary pressure force rapidly decreases. Another consequence of the pressure drop is the increase of the thrust loss (Fig. 8).

The nozzle expansion rate influences the size of the recirculation zone and the plateau pressure level. Two nozzles with the same shadowed ratios, one with a higher and another with a lower expansion rate, cause different side force levels due to different plateau pressures. Nozzles with higher expansion rate have to use a greater shadowed area to achieve the same shadowed ratio.

The influence of the angle of divergence primarily reflects on the position of the oblique shock wave, which is linked with shock flow blocking of the nozzle exit, as above mentioned.

https://doi.org/10.1017/aer.2016.48 Published online by Cambridge University Press

Smaller nozzle divergence angles lead more rapidly to the maximum side force and consequently make this type of TVC more sensitive to shadowing. Therefore, the system becomes less effective.

9.0 CONCLUSION

The paper considers the flow chart modelling of combined thrust vector control research based on the generation of the gas dynamic side force. The research deals with two-dimensional and three-dimensional cold flow tests, some aspects of the real three-dimensional hot flow tests, and CFD simulations of particular phenomena of gas dynamic and geometric relations influencing the design of real TVC systems. The model is developed from the physical behaviour of a supersonic flow constrained by an obstacle in the cone flow conditions. The developed behaviour is adapted for the TVC generation and the consequences of its influence on the intensity and direction of the major thrust force is discussed. The dynamic testing shows a good agreement of the characteristic time gas flow in the recirculation zone as the inertial transformations of transient changes compared with transient time initiated by frequent tab disturbances as the main source of the major disturbed flow phenomena. This comparison could be valid as an average estimation of the unsteady state influences on the guidance process by this flow type of coupled controllers aimed for the TVC on small tactical missiles.

REFERENCES

1. SUTTON, G.P. and BIBLARZ, O. *Rocket Propulsion Elements*, 2001, Wiley, New York, New York, US.
2. OCOKOLJIC, G., ZIVKOVIC, S. and SUBOTIC, S. Aerodynamic coefficients determination for antitank missile with lateral jets, Proceedings of the 4th International Scientific Conference on Defensive Technologies, September 2011, Belgrade, Serbia.
3. GAL-OR, B. Fundamental concepts of vectored propulsion, *Journal of Propulsion and Power*, 1990, **6**, (6), pp 747-757.
4. HUNTER, C.A. and DEERE, K.A. Computational investigation of fluidic counterflow thrust vectoring, Proceedings of the 35th Joint Propulsion Conference and Exhibit, June 1999, Los Angeles, California, US.
5. JOJIC, B., MILINOVIC, M., STEFANOVIC, Z. and BLAGOJEVIC, D. Pressure distribution in rocket nozzle with mechanical system for TVC, Proceedings of the 23rd Joint Propulsion Conference, July 1987, San Diego, California, US.
6. ZIVKOVIC, S. Thrust calculation methods in optimization process for thrust vector system (in Serbian), Proceedings of the 22nd Jugoslovenski Komitet za Eksplozivne Materije, October 2004, Bar, Montenegro.
7. GLIGORIJEVIC, N., ZIVKOVIC, S., SUBOTIC, S., KOZOMARA, S., NIKOLIC, M. and CITAKOVIC, S. Side force determination in the rocket motor thrust vector control system, *Scientific Technical Review*, 2013, **63**, (1), pp 27-38.
8. KOZIC, M. and RISTIC, S. Capability of 2D RANS simulations for 2D thrust vectoring nozzle, *J Aerospace Engineering*, 2010, **224**, (8), pp 905-910.
9. ZIVKOVIC, S., MILINOVIC, M. and ADAMEC, R. Tunnel tests and numerical simulation of the high speed separated nozzle flow, *FME Transactions*, October 2014, **42**, (3), pp 89-97.
10. CHANG, P.K. *Control of Flow Separation: Energy Conservation, Operational Efficiency, and Safety,* Hemisphere Publishing, Washington, DC, US 1976.
11. OSTLUND, J. Flow processes in rocket engine nozzles with focus on flow separation and side-loads, Tech Rep 2002:09, Royal Institute of Technology, Stockholm, 2002.
12. SCHILLING, T.W. Flow Separation in Rocket Nozzles, MS Thesis, University of Buffalo, New York, 1962.

https://doi.org/10.1017/aer.2016.48 Published online by Cambridge University Press

13. WAITHE, K.A. and DEERE, K.A. Experimental and computational investigation of multiple injection ports in a convergent-divergent nozzle for fluidic thrust vectoring, Proceedings of the 21st AIAA Applied Aerodynamics Conference, June 2003, Orlando, Florida, US.
14. TIAN, C. and LU, Y. Turbulence models of separated flow in shock wave thrust vector nozzle, *Engineering Application of Computational Fluid Mechanics*, 2013, **7**, (2), pp 182-192.
15. BALABEL, A., HEGAB, A.M., NASR, M. and EL-BEHERY, S.M. Assessment of turbulence modelling for gas flow in turbulence modelling for gas flow in two-dimensional convergent-divergent rocket nozzle, *Applied Mathematical Modelling*, 2011, **35**, (7), pp 3408-3422.
16. Fluent Incorporated. Fluent 5 User's Guide, 1998, Lebanon, New Hempshire, US.
17. DOBROVOLSKII, V.M. Liquid Rocket Engines (in Russian), Mashinostroenie, Moscow, Russia, 1968.
18. JAUNET, V., AYMER, D., COLLIN, E., BONNET, J.P., LEBEDEV, A. and FOURMENT, C. 3D effects in a supersonic rectangular jet vectored by flow separation control, a numerical and experimental study, Proceedings of the 5th Flow Control Conference, June-July 2010, Chicago, Illinois, US.
19. ZMIJANOVIC, V., RASUO, B. and CHPOUN, A. Flow separation modes and side phenomena in an overexpanded nozzle, *FME Transactions*, September 2012, **40**, (3), pp 111-118.
20. MANGIN, B., CHPOUN, A. and JACQUIN, L. Experimental and numerical study of the fluidic thrust vectoring of a two-dimensional supersonic nozzle, Proceedings of the 24th AIAA Applied Aerodynamics Conference, June 2006, San Francisco, California, US.

https://doi.org/10.1017/aer.2016.48 Published online by Cambridge University Press